Physical Education, Health and Social Sciences

https://journal-of-social-education.org E-ISSN: 2958-5996

P-ISSN: 2958-5988

Elemental Analysis and Plasma Diagnostics of Black Seed Using Laser-Induced Breakdown Spectroscopy

Muhammad Waseem Mirbhar[1], Nek Muhammad Shaikh[2], Altaf Hussain Nizamani[3], Waseem Ahmed Bhutto[4], Saifullah Jamali[5], Muhammad Aslam Khoso[6], Tarique Ali Siyal[7], Zahid Hussain Arain[8], Muhammad Ayaz Khoso[9], Farkhanda Noor[10], Ramsha Saleem[11], Humera Shaikh[12], Meer Hassan Brohi[13]

[1,2,3,4,6, 7,8,9,10,11,12,13,] Institute of Physics, University of Sindh, Jamshoro 71000, Pakistan

[5] Anhui Provincial Key Laboratory of Photonic Devices and Materials, Anhui Institute of Optics and Fine Mechanics, Hefei Institutes of Physical Sciences, Chinese Academy of Sciences, Hefei 230031, China, **Corresponding Author email**: saifjamali86@yahoo.com

DOI: ***https://doi.org/10.63163/jpehss.v4i2.1378***

Abstract

Laser-Induced Breakdown Spectroscopy (LIBS) was employed for elemental analysis and plasma diagnostics of black seed. Plasma was generated using a Q-switched Nd: YAG laser, and emission spectra were recorded over a wide spectral range. The spectral analysis revealed the presence of major elements including C, Mg, Ca, Sr, Na, Ba, H, N, O, K, along with molecular CN bands. The influence of laser energy on plasma characteristics was systematically investigated. Emission intensity was observed to increase with laser energy due to enhanced ablation, excitation, and ionization processes, while slight saturation at higher energies was attributed to plasma shielding effects. Plasma parameters were evaluated to gain deeper insight into plasma behavior. The electron temperature, calculated using the intensity ratio method, varied from ~26,000 K to ~28,000 K with increasing laser energy. The electron number density, determined from Stark broadening of the Hα line, increased from 4.08×10^{17} cm^{-3} to 6.59×10^{17} cm^{-3}. Correspondingly, the plasma frequency was found to increase from 5.75×10^{12} Hz to 7.30×10^{12} Hz. The results demonstrate that LIBS is a rapid, reliable, and effective technique for elemental characterization and plasma diagnostics of agricultural materials, with strong potential for applications in food quality assessment and biomedical studies.

Keywords: Laser-Induced Breakdown Spectroscopy, Black Seed, Elemental Analysis, Plasma Diagnostics, Electron Temperature, Electron Number Density

Introduction

Laser-Induced Breakdown Spectroscopy (LIBS) is an emission-based analytical technique in which a high-energy laser pulse interacts with a material, generating a microplasma whose emission spectrum reveals the elemental composition [1–3]. The performance of LIBS is influenced by several factors, including laser parameters, sample characteristics, and ambient conditions. Owing to its versatility, LIBS has been widely applied in diverse [4-12].

Black seed (*Nigella sativa L.*), commonly known as Kalonji, is a medicinal plant widely recognized for its therapeutic properties, including antioxidant, anti-inflammatory, and

antimicrobial activities. The biological effectiveness and nutritional value of black seed are strongly dependent on its elemental composition. Accurate determination of these elements is therefore important for quality assessment and for understanding its medicinal significance.

Several studies have investigated the elemental composition of plant materials using spectroscopic techniques. For example, Rehan et al. [13] employed LIBS to analyze *Nigella sativa* and reported the presence of multiple elements such as Al, B, Ba, Ca, Cr, K, P, Mg, Mn, Na, Ni, S, Si, Cu, Fe, Ti, Sn, Sr, and Zn. Similarly, Fayyaz et al. [14] applied calibration-free LIBS (CF-LIBS) to *Saussurea simpsoniana* and identified a range of major and trace elements including Al, Ba, C, Ca, Fe, H, K, Li, Mg, Na, Si, Sr, and Ti. In addition, Abubakar et al. [15] used atomic absorption spectroscopy to and reported Zn, Fe, Cu, Mg, Ca, Na, and K in black seed and jujube. These studies demonstrate the importance of elemental profiling; however, the composition of seeds can vary significantly depending on environmental factors such as soil composition, water quality, and geographical location. Despite these contributions, comprehensive LIBS studies focusing on both elemental analysis and plasma diagnostics of locally grown black seed remain limited. In particular, the effect of laser energy on plasma characteristics and its correlation with emission behavior has not been thoroughly investigated. Addressing this gap is essential for improving the accuracy and applicability of LIBS in agricultural and biomedical studies.

Therefore, the aim of the present study is to perform detailed elemental analysis and plasma diagnostics of black seed using LIBS. The emission spectra are analyzed to identify major and trace elements, while the effect of laser energy on plasma characteristics is systematically examined. Furthermore, key plasma parameters, including electron temperature, electron number density, and plasma frequency, are evaluated to provide a comprehensive understanding of plasma dynamics. This integrated approach enhances the analytical potential of LIBS and supports its application in food quality assessment and related fields.

Experimental Setup

The experimental setup, as depicted in Fig. 1, utilized Second Harmonic Generation (SHG) at 532 nm from a Q-switched Nd:YAG laser (Quantel Brilliant) with a 5 ns pulse duration and a repetition rate of 10 Hz. The laser beam was focused onto the target at atmospheric pressure using a 20 cm quartz lens. To avoid cratering, the plasma emission spectra were captured on a pristine surface. The emitted light from the plasma was detected using the LIBS2000 system (Ocean Optics, Inc.), coupled with an optical fiber (high OH, 600 μm core diameter, and a collimating lens with a 0–45° field of view), positioned perpendicular to the plasma expansion direction. The LIBS2000 detection system comprises five individual spectrometers, each equipped with a 5 μm slit width, covering a total wavelength range from 200 nm to 720 nm. Each spectrometer features a linear CCD array with a resolution of 2048 elements and an optical resolution of 0.1 nm. The synchronization of the Nd:YAG laser and the LIBS2000 system was achieved using a four-channel digital delay/pulse generator (SRS DG535). The data from all spectrometers were simultaneously collected and stored on a PC for subsequent analysis using the OOI LIBS software.

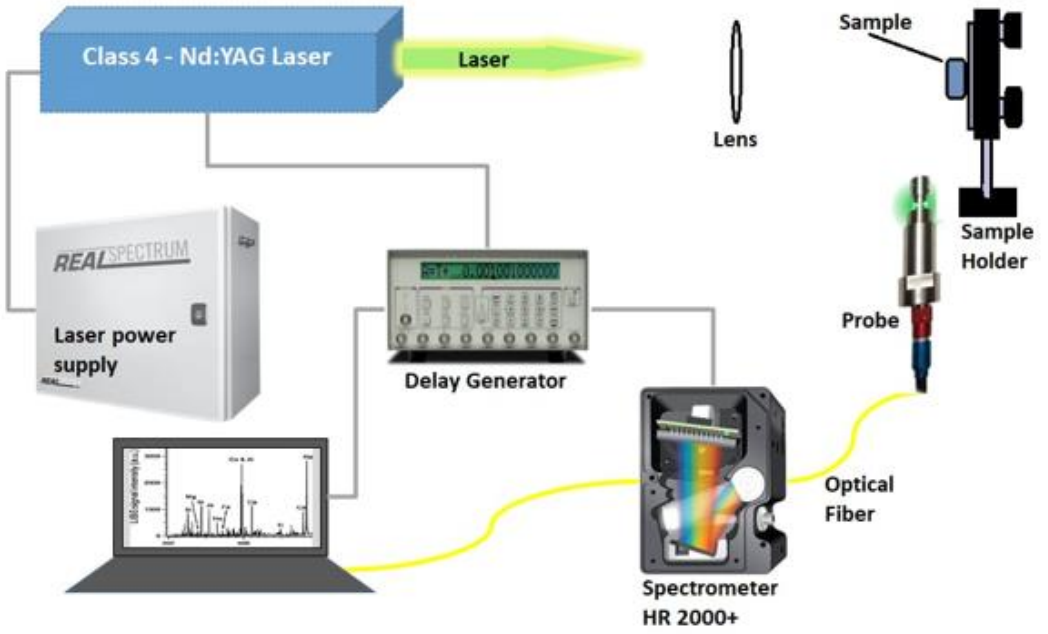

Fig. 1 LIBS experimental setup [16]

Results and Discussion:

Emission Spectral Analysis

The emission spectra of laser-induced plasma from black seed were recorded. The spectra reveal the presence of several neutral and singly ionized atomic lines along with molecular bands, indicating the complex elemental composition of the sample. Fig. 2(a), covering the spectral region from 225 to 287 nm, shows a prominent neutral carbon line (C I) at 247.85 nm and a neutral magnesium line (Mg I) at 285.21 nm. In addition, four strong singly ionized magnesium lines (Mg II) are observed at 279.07 nm, 279.79 nm, 279.80 nm, and 280.27 nm, indicating significant plasma excitation and ionization. In Fig. 2(b) (310–390 nm), two singly ionized calcium lines (Ca II) at 315.88 nm and 317.93 nm are identified, along with neutral magnesium lines at 383.23 nm and 383.82 nm. The presence of the CN molecular band in this region suggests recombination processes occurring within the cooling plasma plume. Figure 2(c) illustrates the spectral range containing prominent Ca II lines at 393.36 nm and 396.84 nm, along with a neutral calcium line (Ca I) at 422.67 nm. A strontium line (Sr I) at 407.77 nm is also detected, indicating trace elemental presence. The coexistence of neutral and ionic lines reflects partial ionization conditions in the plasma. The spectral region shown in Fig. 2(d) includes three strong neutral magnesium lines at 516.73 nm, 517.26 nm, and 518.36 nm. Additionally, sodium-related emissions (Na I) are observed around 526 nm. A distinct line at 532 nm corresponds to the second harmonic of the Nd:YAG laser, while a neutral calcium line appears at 558.87 nm. In Fig. 2(e), multiple neutral calcium lines are observed at 585.74 nm, 610.27 nm, and 612.22 nm, along with prominent sodium doublet lines at 588.99 nm and 589.59 nm. A weak barium line (Ba I) at 611.07 nm is also detected, suggesting minor elemental contributions. Figure 2(f) shows neutral calcium lines at 643.90 nm and 714.81 nm. A strong hydrogen alpha (H I) emission line is observed at 656.28 nm, which is commonly used for plasma diagnostics. Additionally, neutral nitrogen lines are identified at 742.36 nm,

744.22 nm, and 746.83 nm. In Fig. 2(g), two strong potassium resonance lines (K I) are observed at 766.49 nm and 769.89 nm. Oxygen lines (O I) are detected at 777.29 nm and 795.08 nm. The dominance of nitrogen emission lines in this region is attributed to interactions between the plasma and ambient air. Fig. 2(h) is dominated by multiple neutral nitrogen lines in the range of 856–873 nm, indicating strong plasma–air interaction. A singly ionized calcium line (Ca II) is also observed at 866.21 nm. Finally, Fig. 2(i) shows additional nitrogen lines at 938.68 nm, 939.27 nm, and 946.06 nm, along with an oxygen line at 926.60 nm. Overall, the spectral analysis confirms the presence of C, Mg, Ca, Sr, Na, Ba, H, N, O, K and CN band in black seed. The coexistence of neutral and ionic species, along with molecular emissions, indicates that the plasma is in a transient state with ongoing excitation, ionization, and recombination processes.

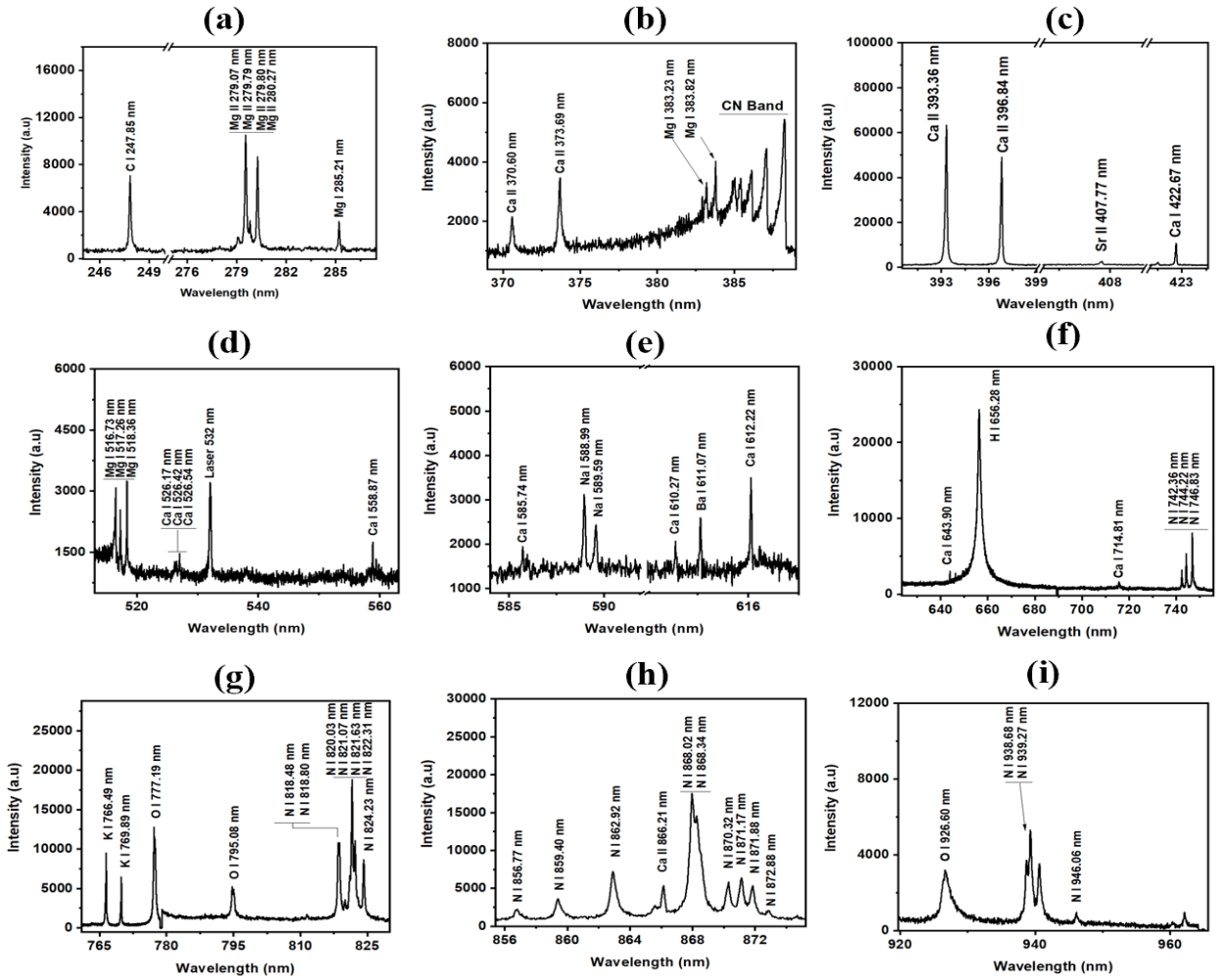

Fig 2. (a-i) Emission spectra of black seed plasma

Effect of Laser Energy on Emission Intensity

The characteristics of laser-induced plasma are strongly governed by the incident laser energy, which directly influences plasma formation, temperature, electron density, and degree of ionization. As the laser pulse interacts with the sample surface, its energy is absorbed, leading to rapid heating, melting, vaporization, and subsequent ionization of the ablated material.

Consequently, the variation in laser energy significantly affects the emission intensity and spectral features of the plasma. At lower laser energies, insufficient energy deposition results in weak ablation and incomplete plasma formation. This leads to reduced excitation of atomic species and consequently weak emission lines. As the laser energy increases, a larger of material is ablated, producing a denser plasma plume with higher electron temperature and electron number density. This enhances collisional excitation and ionization processes, resulting in stronger emission intensities. Fig. 3 illustrates the three-dimensional variation of spectral intensity as a function of laser energy and delay time. It is observed that the emission intensity increases with increasing laser energy. This behavior can be attributed to increased plasma temperature and improved population of excited states at higher energies. Additionally, optimal delay times allow detection of emission after continuum radiation decays, thereby improving signal-to-background ratio.

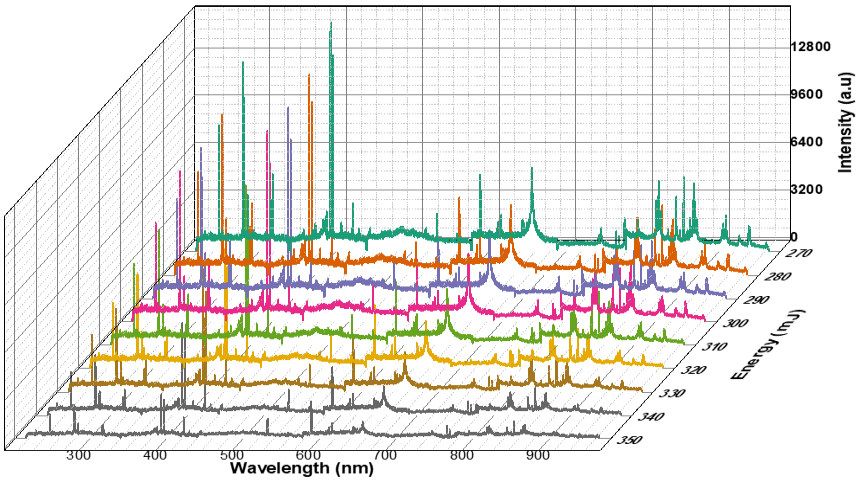

Fig 3. 3D spectral variation along with different energy

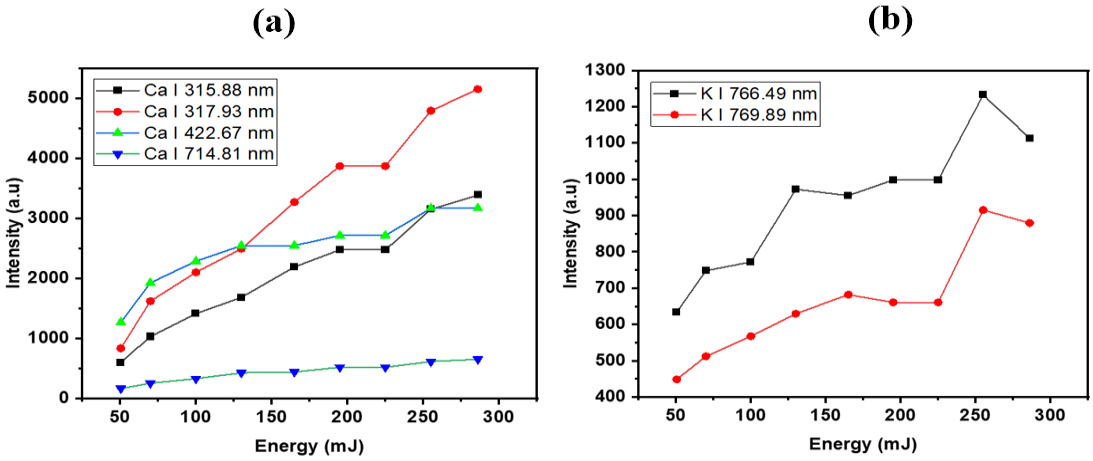

Fig 4. (a-b) Variation of emission intensity with laser energy.

Fig. 4(a–b) shows the variation of emission intensities of selected Ca and K spectral lines with laser energy. A clear increasing trend in line intensity is observed with increasing laser energy. This enhancement is primarily due to increased ablation rate, higher electron temperature, and enhanced electron density. However, at very high laser energies, the rate of increase in emission

intensity may become less pronounced due to plasma shielding effects. In this phenomenon, the dense plasma formed at early stages absorbs and scatters the incoming laser radiation, thereby reducing the effective energy reaching the target surface.

Electron Temperature

The electron temperature of the laser-induced plasma was determined using the intensity ratio method under the assumption of local thermodynamic equilibrium (LTE). This method is based on the Boltzmann distribution, which relates the population of excited states to the plasma temperature. The electron temperature can be calculated using the following relation [17].

$$T = \frac{E_1 - E_2}{k \ln\left(\frac{g_1 A_1 \lambda_2 I_2}{g_2 A_2 \lambda_1 I_1}\right)}$$

where E_1 and E_2 are the upper energy levels of the selected transitions, g represents the statistical weight, A is the transition probability, λ is the wavelength, I is the measured line intensity, and k is Boltzmann's constant. For this study, two Mg II emission lines at 279.07 nm and 279.80 nm were selected due to their high intensity and minimal spectral interference. The relevant spectroscopic parameters were used to calculate the electron temperature. The calculated electron temperature for the black seed plasma ranges from ~26,000 K at 165 mJ to ~28,000 K at 345 mJ, as shown in Fig. 5.

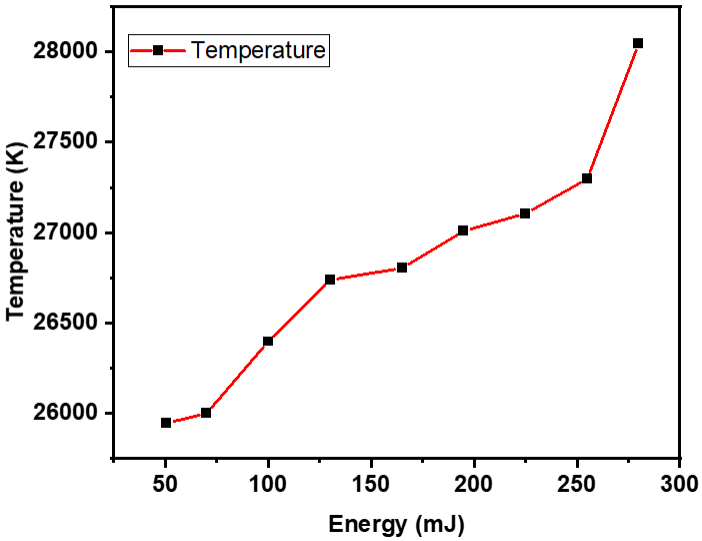

Fig. 5 Variation of electron temperature at different energy.

The increase in electron temperature with laser energy is attributed to enhanced energy deposition into the plasma. At higher laser energies, a larger amount of material is ablated, resulting in increased electron density and more frequent electron–atom collisions. These processes improve excitation efficiency and promote population of higher energy states, leading to an increase in plasma temperature. Additionally, higher laser energy contributes to stronger plasma confinement and reduced relative energy losses, further supporting the observed temperature rise. The obtained temperature values are consistent with typical LIBS plasma conditions, confirming the reliability of the applied method.

Electron Number Density

The electron number density (N_e) of the laser-induced plasma was determined using the Stark broadening of the hydrogen alpha (H I) spectral line at 656.28 nm. Stark broadening is one of the most reliable methods for electron density estimation in LIBS plasma, as the broadening of spectral lines is primarily caused by interactions between emitting species and surrounding charged particles, particularly electrons. The full width at half maximum (FWHM), denoted as $\Delta\lambda_{1/2}$, of the Hα line was extracted by fitting the experimental spectral profile with a Lorentzian function using OriginPro software. The electron number density was then calculated using the Stark broadening relation [17].

$$N_e = \left(\frac{\Delta\lambda_{FWHM}}{1.098}\right)^{1.473} \times 10^{17} cm^{-3}$$

where $\Delta\lambda_{1/2}$is the measured FWHM of the spectral line, $\omega$is the electron impact parameter (Stark broadening coefficient), and $N_e$is the electron number density in cm^{-3}. The calculated electron number density for the black seed plasma was found to increase from 4.08 × 10^{17} cm^{-3} at 50.5 mJ to 6.59 × 10^{17} cm^{-3} at 255 mJ, as shown in Fig. 6.

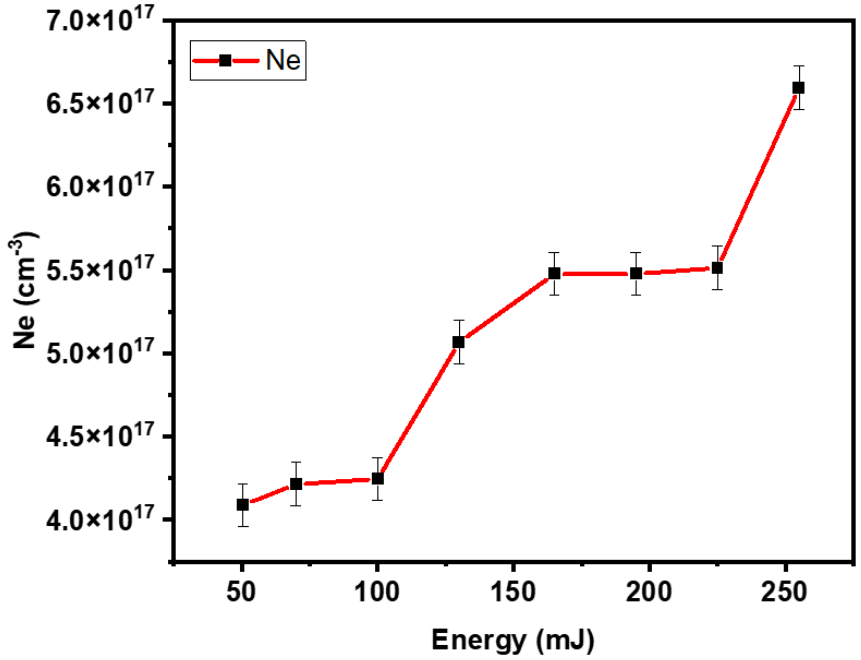

Fig. 6 variation of electron number density at different energy.

The observed increase in electron number density with laser energy can be attributed to enhanced ablation and ionization processes. At higher laser energies, a larger amount of material is vaporized, leading to increased plasma density and a higher concentration of free electrons. This results in stronger electron–ion interactions, which broaden the spectral lines and reflect higher electron densities. Additionally, the increase in $N_e$indicates more efficient plasma formation and stronger collisional processes at elevated laser energies. The obtained electron density values are within the typical range for LIBS plasma, confirming the validity of the applied Stark broadening method.

Plasma Frequency

Following laser–matter interaction, a transient plasma plume is generated consisting of electrons, ions, and neutral species. The collective oscillation of free electrons within this plasma is characterized by the plasma frequency, which is a fundamental parameter describing the dynamic behavior of charged particles. The plasma frequency is directly related to the electron number density and can be expressed as [17].

$$\omega_p = 9 \times 10^3 \sqrt{N_e}$$

where $\omega_p$is the plasma frequency (Hz) and $N_e$is the electron number density (cm^{-3}). In this study, the electron number density obtained from Stark broadening of the hydrogen alpha (H I) line at 656.28 nm was used to estimate the plasma frequency. The calculated plasma frequency was found to increase from 5.75 × 10^{12} Hz at 50.5 mJ to 7.30 × 10^{12} Hz at 255 mJ, as illustrated in Fig. 7.

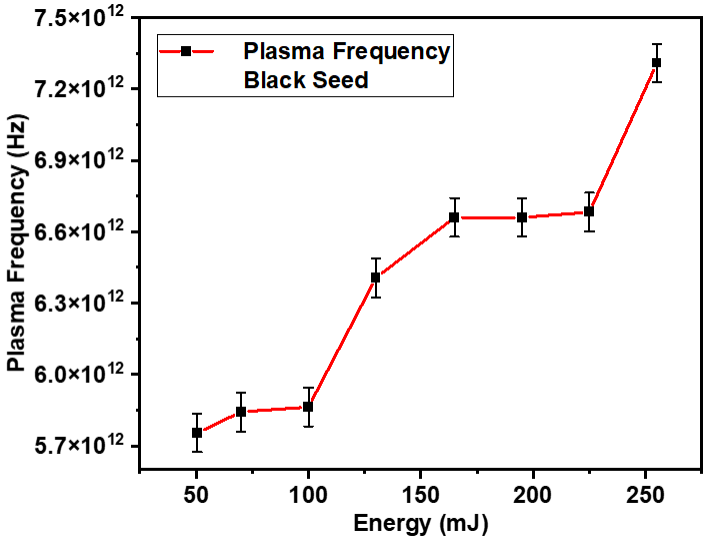

Fig. 7 Variation of plasma frequency with laser energy.

The increase in plasma frequency with laser energy is directly associated with the rise in electron number density. At higher laser energies, enhanced ablation and ionization processes generate a greater population of free electrons within the plasma plume. This leads to stronger collective oscillations of electrons, resulting in higher plasma frequency values. Moreover, the observed trend indicates improved plasma coupling and higher energy absorption efficiency at elevated laser energies. Since plasma frequency governs the interaction of electromagnetic radiation with plasma, its increase also reflects a denser and more conductive plasma state. The obtained plasma frequency values are consistent with typical LIBS plasma conditions, confirming the reliability of the diagnostic approach used in this study.

Conclusion

In this study, Laser-Induced Breakdown Spectroscopy (LIBS) was successfully utilized for elemental analysis and plasma diagnostics of black seed. The emission spectra recorded over the range of 190–960 nm revealed the presence of major elements such as C, Mg, Ca, Sr, Na, Ba, H,

N, O, K and molecular CN bands, confirming the complex elemental composition of the sample. The effect of laser energy on plasma characteristics was systematically investigated. It was observed that emission intensity increases with increasing laser energy due to enhanced ablation, excitation, and ionization processes, while slight deviations at higher energies were attributed to plasma shielding effects. Plasma diagnostics showed that the electron temperature increased from ~26,000 K to ~28,000 K with increasing laser energy, indicating stronger excitation and energy coupling within the plasma. The electron number density, calculated using Stark broadening of the Hα line, increased from 4.08×10^{17} cm^{-3} to 6.59×10^{17} cm^{-3}, reflecting enhanced ionization and plasma density. Correspondingly, the plasma frequency also increased, confirming the strong dependence of plasma dynamics on electron density. Overall, the results demonstrate that LIBS is an effective and reliable technique for both elemental characterization and plasma diagnostics of agricultural materials. The findings of this study provide valuable insights into plasma behavior and highlight the potential of LIBS for applications in food quality assessment, agricultural analysis, and biomedical research.

Acknowledgement
All Authors are thankful to Quaid-e-Azam University, Islamabad, for providing the necessary experimental facilities in the atomic and molecular physics laboratory.

Reference:

Song, X., Li, K., Dai, K., Wang, X., Du, H., & Zhao, H. (2022). A random-forest-assisted artificial neural network method for analysis of steel using laser-induced breakdown spectroscopy. *Optik, 249*, 168214. https://doi.org/10.1016/j.ijleo.2021.168214

Zhao, S., Afgan, M. S., Zhu, H., & Gao, X. (2022). Femtosecond laser filamentation-induced breakdown spectroscopy combined with chemometric methods for soil heavy metals analysis. *Optik*, 251, 168444. https://doi.org/10.1016/j.ijleo.2021.168444

Jamali, S., Shaikh, N. M., Khoso, M. A., Jamil, Y., Bhutto, W. A., Soomro, A. M., & Mari, R. H. (2022). Elemental analysis of talcum powder using spectroscopic techniques. *Optik*, 261, 169246. https://doi.org/10.1016/j.ijleo.2022.169246

Shaikh, N. M., Rashid, B., Hafeez, S., Jamil, Y., & Baig, M. A. (2006). Measurement of electron density and temperature of a laser-induced zinc plasma. *Journal of Physics D: Applied Physics*, 39, 1384–1391. https://doi.org/10.1088/0022-3727/39/7/008

Lednev, V. N., Sdvizhenskii, P. A., Stavertiy, A. Y., Grishin, M. Y., Tretyakov, R. S., Asyutin, R. D., & Pershin, S. M. (2021). Online and in situ laser-induced breakdown spectroscopy for laser welding monitoring. *Spectrochimica Acta Part B: Atomic Spectroscopy*, 175, 106032. https://doi.org/10.1016/j.sab.2020.106032

Zeng, Q., Sirven, J. B., Gabriel, J. C. P., Tay, C. Y., & Lee, J. M. (2021). Laser-induced breakdown spectroscopy for plastic analysis. *TrAC Trends in Analytical Chemistry*, 140, 116280. https://doi.org/10.1016/j.trac.2021.116280

Costa, V. C., et al. (2018). Novel LIBS method for micro-spatial chemical analysis of inorganic gunshot residues. *Journal of Chemometrics*, 32, e3208. https://doi.org/10.1002/cem.3208

Bol'shakov, A. A., Yoo, J. H., Liu, C., Plumer, J. R., & Russo, R. E. (2010). Laser-induced breakdown spectroscopy in industrial and security applications. *Applied Optics*, 49, C132–C142. https://doi.org/10.1364/AO.49.00C132

Jamali, S., Khoso, M. A., Zaman, M. H., Jamil, Y., Bhutto, W. A., Abbas, A., Mari, R. H., Kalhoro, M. S., & Shaikh, N. M. (2021). Elemental analysis using laser ablation and atomic absorption spectroscopy techniques. *Physica B: Condensed Matter*, 620, 413278. https://doi.org/10.1016/j.physb.2021.413278

Ashraf, M., Shaikh, N. M., Kandhro, G. A., Murtaza, G., Iqbal, J., Iqbal, A., & Lashari, S. A. (2020). Energy penetration and inverse bremsstrahlung absorption coefficient in laser-ablated germanium plasma. *Journal of Molecular Structure*, 1203, 127412. https://doi.org/10.1016/j.molstruc.2019.127412

Farooq, W. A., Al-Johani, A. S., Alsalhi, M. S., Tawfik, W., & Qindeel, R. (2020). Analysis of polystyrene and polycarbonate used in manufacturing of water and food containers using laser-induced breakdown spectroscopy. *Journal of Molecular Structure*, 1201, 127152. https://doi.org/10.1016/j.molstruc.2019.127152

Zhang, Y., Zhang, T., & Li, H. (2021). Application of laser-induced breakdown spectroscopy in environmental monitoring. *Spectrochimica Acta Part B: Atomic Spectroscopy*, 181, 106218. https://doi.org/10.1016/j.sab.2021.106218

Rehan, I., Khan, M. Z., Ali, I., Rehan, K., Sultana, S., & Shah, S. (2018). Spectroscopic analysis of high protein nigella seeds (Kalonji) using laser-induced breakdown spectroscopy and inductively coupled plasma/optical emission spectroscopy. *Applied Physics B*, 124, 49. https://doi.org/10.1007/s00340-018-6915-z

Fayyaz, A., Ali, N., Umar, Z. A., Asghar, H., Waqas, M., Ahmed, R., Ali, R., & Baig, M. A. (2024). CF-LIBS based elemental analysis of *Saussurea simpsoniana* medicinal plant: A study on roots, seeds, and leaves. *Analytical Sciences*, 40, 413–427. https://doi.org/10.1007/s44211-023-00480-9

Abubakar, H. B., Falaki, F. A., Suleiman, H. I., Sufyan, A. J., Jibril, M. M., Idi, A., Musa, K. A., Babandi, A., & Yakasai, H. M. (2023). Proximate and elemental composition of black seed and jujube as formulation for the treatment of peptic ulcer. *Journal of Environmental Bioremediation and Toxicology*, 6(1), 19–23. https://doi.org/10.54987/jebat.v6i1.810

Jamali, S., Shaikh, N. M., Zhang, Z., Fu, H., Bhutto, W. A., Soomro, A. M., Siyal, T. A., Sanjrani, I. A., Soomro, A., Saleem, R., & Khoso, M. A. (2026). Laser induced breakdown spectroscopy for elemental profiling and plasma diagnostics of cosmetic products. *Pakistan Journal of Chemistry*, 16(1–2), 38–44. https://doi.org/10.15228/2026.v16.i1-2.p.38-44

Jamali, S., Khoso, M. A., Zaman, M. H., Jamil, Y., Bhutto, W. A., Abbas, A., Mari, R. H., Kalhoro, M. S., & Shaikh, N. M. (2021). Elemental analysis of kohl using laser ablation and atomic absorption spectroscopy techniques. *Physica B: Condensed Matter*, 620, 413278. https://doi.org/10.1016/j.physb.2021.413278